Chinese Chemical Letters 37 (2026) 111785

Contents lists available at ScienceDirect

Chinese Chemical Letters

journal homepage: www.elsevier.com/locate/cclet

Boosting alkaline hydrogen evolution kinetics in CoP *via* high-valence ion doping for anion exchange membrane electrolyzers

Shiqing Zhang[a,b], Zihao Wang[a,b], Shaokai Ma[a,b], Zihang Cao[a,b], Fang Liu[a,b], Ying Li[a], Xuewen Xu[a,b], Yuanhui Ma[a,b], Yanming Xue[a,b], Chengchun Tang[a,b], Jun Zhang[a,b,*]

[a] School of Material Science and Engineering, Hebei University of Technology, Tianjin 300130, China
[b] Hebei Key Laboratory of Boron Nitride Micro and Nano Materials, Tianjin 300130, China

ARTICLE INFO

Article history:
Received 18 June 2025
Revised 7 August 2025
Accepted 2 September 2025
Available online 2 September 2025

Keywords:
CoP
Electronic structure
Water dissociation
Adsorption free energy
AEM electrolyzer

ABSTRACT

Advancing low-cost and efficient electrocatalysts for the hydrogen evolution reaction (HER) in alkaline media is essential for sustainable hydrogen production, particularly in the context of anion exchange membrane (AEM) water electrolysis systems. Among various candidates, cobalt-based phosphides, particularly CoP, have drawn significant attention as cost-effective alternatives to platinum-based HER electrocatalysts due to their excellent catalytic performance. However, improving both water dissociation kinetics and hydrogen adsorption free energies remains a challenge. In this study, we introduce lead (Pb), a non-transition metal with higher electronegativity and a similar ionic radius to Co, to modify the electronic structure of CoP at both Co and P sites. Pb doping significantly optimizes both water dissociation and adsorption free energy in the alkaline HER process. The optimized Pb-CoP/CC electrocatalyst reduces the overpotential from 100 mV to 53 mV and achieves a Tafel slope of 57 mV/dec in alkaline electrolyte. Additionally, it exhibits excellent durability, maintaining stable performance for over 120 h. The improved HER performance of Pb-CoP/CC can be ascribed to the synergistic interactions between its components: accelerated water dissociation on Co sites, optimized hydrogen intermediate adsorption on P sites, and improved charge transfer abilities. These findings are supported by experimental data and DFT calculations. When used as the cathode in an AEM electrolyzer, Pb-CoP/CC achieves a current density of 500 mA/cm^2 at 1.95 V, demonstrating excellent stability. This work highlights the efficacy of metal ion doping with higher electronegativity in improving HER performance and establishes a versatile strategy for other non-precious metal-based transition metal compounds, paving the way for high-performance AEM electrolyzers.

© 2026 Published by Elsevier B.V. on behalf of Chinese Chemical Society and Institute of Materia Medica, Chinese Academy of Medical Sciences.

Converting renewable energy into hydrogen represents one of the most promising approaches to mitigate the global energy crisis and reduce environmental pollution [1–4]. Among various hydrogen production technologies, water electrolysis using anion exchange membrane (AEM) electrolyzers has gained significant attention due to its combined advantages of proton exchange membrane (PEM) and alkaline water electrolysis systems [5–7]. An AEM electrolyzer consists of a cathode and an anode, with the hydrogen evolution reaction at the cathode being a key challenge due to its high reaction energy barrier and sluggish kinetics [8–10]. To overcome this limitation, efficient electrocatalysts are required to accelerate the HER process [11,12]. Currently, Pt-based noble metal catalysts are considered the benchmark for HER due to their exceptional activity and stability [13]. However, the scarcity and high cost of Pt severely limit its widespread application [14]. Consequently, non-noble metal-based catalysts have emerged as promising alternatives [15].

Among these, NiMo-based catalysts have been extensively studied and exhibit excellent catalytic performance under the alkaline condition of AEM electrolysis [11,16–20]. However, the use of expensive Mo and the complexities associated with bimetallic systems remain challenges [21]. In this context, Co-based monometallic compounds, such as transition metal phosphides, sulfides, and selenides, have garnered significant attention as cost-effective and efficient alternatives [22]. Particularly, cobalt phosphides (CoP) have shown comparable activity and stability to Pt and NiMo-based catalysts, owing to its unique hydrogenase-like structure, making them highly attractive for HER in AEM electrolyzers [23–28]. As known, both cobalt (Co) and phosphorus (P) sites function as active centers for the HER under acidic conditions, with Co

* Corresponding author.
E-mail address: zhang.jun@hebut.edu.cn (J. Zhang).

https://doi.org/10.1016/j.cclet.2025.111785
1001-8417/© 2026 Published by Elsevier B.V. on behalf of Chinese Chemical Society and Institute of Materia Medica, Chinese Academy of Medical Sciences.

serving as hydride acceptors and P as proton acceptors [29–31]. Such synergistic interaction significantly enhances the catalytic activity in acidic environments. However, under alkaline conditions, CoP suffers from reduced catalytic activity due to the sluggish kinetics of water dissociation at the beginning of the HER, making the enhancement of water dissociation a key factor in improving its alkaline HER performance [32–35]. Therefore, optimizing both the water dissociation energy and the hydrogen adsorption free energy of intermediates is crucial for enhancing the hydrogen evolution performance of CoP under alkaline conditions [36].

Previous studies have shown that under alkaline conditions, the positively charged Co sites preferentially adsorb and dissociate water, while the resulting H ions are transferred to the negatively charged P sites to combine and produce hydrogen [32–34,37,38]. Therefore, modifying the electronic structure of CoP is critical for enhancing water dissociation and hydrogen adsorption energy, thereby improving alkaline HER performance [39]. Raising the oxidation state of Co to improve water adsorption and dissociation can be achieved through various strategies, such as vacancy engineering, doping, and composite formation [34,40–42]. Among these strategies, doping is particularly effective [43], as it can simultaneously modulate both Co and P sites, improving water dissociation and/or optimizing hydrogen adsorption energy [33,35]. Typically, anion doping is employed to regulate the electronic structure of metal Co sites, enhancing water dissociation capability. However, it is important to note that anion doping has a minimal impact on the electronic structure of the P site. Moreover, replacing P sites with anions inevitably reduces the number of active sites available for hydrogen adsorption, which can adversely affect the overall catalytic activity. In contrast, cation doping can modulate the electronic structure of both Co and P sites without reducing the number of active P sites. To improve the oxidation state of Co, doping with high-valence or highly electronegative metal ions, such as Mo, W, Zr, and Cr, is more effective in tuning the electronic structure of CoP, thereby enhancing its catalytic activity [44–47]. However, there are few reports discussing strategies that can simultaneously increase the Co oxidation state and decrease the P oxidation state through cation doping. In addition, the use of transition metal dopants complicates the identification of active sites, highlighting the need for non-transition metal dopants that can improve water dissociation by raising the valence state of Co while enhancing hydrogen adsorption by lowering the valence state of P [48–50]. As a typical non-transition metal, Pb, with its higher electronegativity (2.33) compared to Co (1.88) and an ionic radius (84 pm) similar to that of Co (74 pm), is an ideal dopant for this purpose. Pb doping may effectively modulate the electronic structure of CoP, enhancing both water dissociation and intermediate adsorption during the alkaline hydrogen evolution reaction. Notably, Pb-doped CoP for alkaline HER has not yet been reported.

Herein, Pb-doped CoP nanowires self-supported on carbon cloth (Pb-CoP/CC) have been strategically designed and synthesized as an efficient HER electrocatalyst. Compared to pristine CoP/CC, the optimized Pb-CoP/CC catalyst exhibits a reduced overpotential of 53 mV at 10 mA/cm^2 and a Tafel slope of 57 mV/dec, with excellent stability over 120 h. Both experimental and theoretical results confirm that Pb doping enhances water dissociation, hydrogen adsorption, and interface charge transfer abilities, leading to superior catalytic performance. Moreover, the Pb-CoP/CC cathode, paired with a commercial IrO_2-loaded Pt-Ti felt, demonstrates high performance and durability in an AEM electrolyzer, achieving a cell voltage of 2.58 V at 500 mA/cm^2. This study highlights the potential of non-transition metal doping to modulate the electronic structure of non-noble metal catalysts to effectively optimize both water dissociation and free energy adsorption, paving the way for the industrial application of AEM electrolyzers.

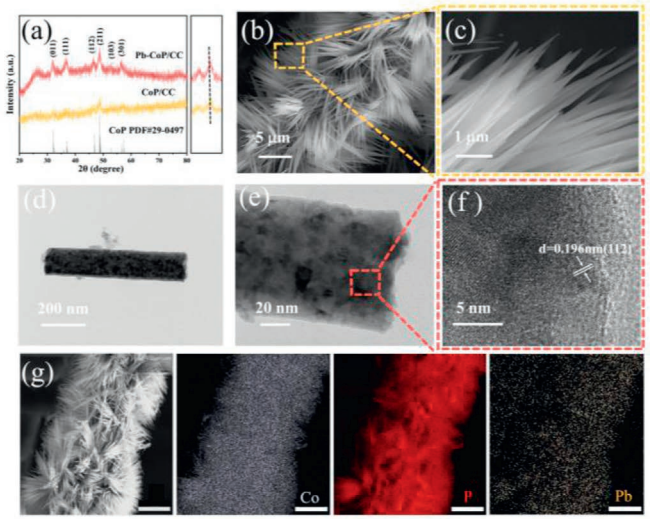


Fig. 1. (a) XRD patterns of the synthesized CoP/CC and Pb-CoP/CC samples. (b, c) The SEM images of Pb-CoP/CC at varied magnifications. (d) TEM and (e, f) HRTEM images of Pb-CoP/CC. (g) EDS mapping of Pb-CoP/CC.

As depicted in Scheme S1 (Supporting information), the synthesis of Pb-CoP/CC on carbon cloth follows a two-step process. First, Pb-$Co(OH)_2$/CC is grown on the carbon cloth *via* a simple hydrothermal method. This is followed by a low-temperature phosphating step to produce Pb-CoP/CC. The doping level is precisely controlled by varying the amount of $PbCl_2$ used during the hydrothermal process. The crystal structure and phase properties of all the obtained samples were analyzed using by X-ray diffraction (XRD). Fig. S1 (Supporting information) shows the XRD patterns of $Co(OH)_2$/CC and Pb-$Co(OH)_2$/CC precursors. The results reveal relatively modest crystallinity, yet the patterns closely match the standard reference for $Co(OH)_2$ (JCPDS No. 48-83). As shown in Fig. 1a, the XRD spectra of Pb-CoP/CC closely resemble those of CoP reported in the JCPDS database (JCPDS No. 29-0497). Distinct diffraction peaks are observed at 32.7°, 37.4°, 46.8°, 49.1°, 52.8°, and 58.2°, corresponding to the (011), (111), (112), (211), (103), and (301) crystal planes of CoP, respectively. Notably, the incorporation of Pb into CoP results in increased peak intensity, indicating enhanced crystallinity of CoP after Pb doping. Additionally, the diffraction peak corresponding to the (211) crystal plane in Pb-CoP/CC shifts slightly towards smaller angles compared to undoped CoP, suggesting lattice expansion in CoP due to Pb incorporation and supporting the possibility of Pb doping within the CoP/CC lattice. All the aforementioned XRD results confirm the successful formation of CoP/CC by converting the $Co(OH)_2$/CC precursor through the adopted phosphating process, as well as the possible doping of Pb into the CoP lattice.

To further investigate the surface features and internal structure of the material, scanning electron microscopy (SEM) and transmission electron microscopy (TEM) were used for observation and analysis. Fig. S2 (Supporting information) presents the SEM images of the $Co(OH)_2$/CC and Pb-$Co(OH)_2$/CC precursor materials, which were *in situ* grown on carbon cloth. Both samples display similar nanowire array structures with lengths of approximately 10 μm, indicating that Pb ion doping does not alter the morphology of $Co(OH)_2$/CC. In the CoP/CC sample, the nanowires exhibit a relatively compact bundle arrangement (Fig. S3 in Supporting information), which is favorable for electrolyte infiltration and reactant transport. After Pb doping, Pb-CoP/CC retains the basic nanowire array structure, but the arrangement of the nanowires becomes looser and more ordered (Figs. 1b and c), consistent with the lattice modulation evidenced by the XRD results. The

XRD and SEM results of CoP/CC and Pb-CoP/CC suggest that while Pb doping may have a negative impact on the catalytic active sites of CoP, while it is beneficial for improving its catalytic stability. The low-magnification TEM image in Fig. 1d confirms the nanowire-like structure of Pb-CoP/CC, consistent with the SEM results described above. Additionally, the high-resolution transmission electron microscopy (HRTEM) images in Figs. 1e and f reveal a lattice spacing of 0.196 nm for Pb-CoP/CC, corresponding to the (112) crystal plane of CoP, which aligns well with the XRD observations. Energy-dispersive X-ray spectroscopy (EDS) analysis (Fig. 1g) confirms the presence and uniform distribution of Co, P, and Pb elements in the Pb-doped CoP nanowires, further supporting the successful incorporation of Pb atoms into the CoP crystal lattice. The atomic percentages of Co, P, and Pb in Pb-CoP/CC are approximately 46.25 %, 52.99 %, and 0.76 %, respectively (Fig. S4 in Supporting information). The introduction of Pb into CoP is anticipated to modify the oxidation states and electronic structures of the surrounding elements, thereby modulating the intrinsic catalytic activity for the hydrogen evolution reaction.

Raman spectroscopy was performed on Pb-CoP/CC to further verify the incorporation of Pb into the crystal lattice. As shown in Fig. S5 (Supporting inormation), Pb-CoP/CC retains similar characteristic vibrational modes to those of CoP/CC, indicating that the fundamental crystal structure is preserved. However, a distinct blue shift of the characteristic peak at 489 cm^{-1} is observed. This shift originates from the partial substitution of Co by Pb, which enhances the bond strength of Co-P and increases the vibrational frequency, thereby confirming the successful doping of Pb. This alteration in the local bonding environment directly affects the electronic structure of the material, subsequently modulating its catalytic performance.

To gain a more comprehensive understanding of the elemental composition and chemical valence states of Co and P in CoP/CC and Pb-CoP/CC, X-ray photoelectron spectroscopy (XPS) analysis was conducted for all elements present in the samples. As shown in Fig. 2a, the spectra of CoP/CC and Pb-CoP/CC indicate a uniform distribution of Co, P, and C elements. Additionally, the Pb-CoP/CC spectrum exhibits a distinct Pb signal around 140 eV, corresponding to a doping level of approximately 0.71 % (Table S1 in Suporting information), consistent with the EDS results. The slight difference in Pb content between EDS (0.76 at%) and XPS (0.71 at%) is due to their different detection depths. This variation is within an acceptable range and both confirm successful Pb doping. In the Co 2p orbital spectrum in CoP/CC (Fig. 2b), the two main peaks at 778.2 and 793.1 eV correspond to Co $2p_{3/2}$ and Co $2p_{1/2}$, respectively, and are attributed to Co^0 [51]. On the other hand, the second set of peaks at 781.5 eV in the Co $2p_{3/2}$ region and 797.7 eV in the Co $2p_{1/2}$ region are assigned to oxidized Co species ($Co^{2+/3+}$). Additionally, two satellite peaks at 784.6 and 802.4 eV are identified through deconvolution. Notably, the introduction of Pb ions induces a slight shift in the binding energy of Co^0 toward higher values, indicating that Pb incorporation alters the electron density of Co in Pb-CoP/CC, resulting in a more positive charge. This change results in an increased oxidation state, which could enhance the catalyst's water dissociation capability [32]. In the P 2p spectrum in CoP/CC (Fig. 2c), the peaks at 130.9 eV and 129.7 eV correspond to the P $2p_{1/2}$ and P $2p_{3/2}$ levels, respectively, while the peak at 134.7 eV is attributed to oxidized phosphorus. After Pb doping, the binding energy peaks of P $2p_{3/2}$ and P $2p_{1/2}$ shift towards lower energies, indicating that the phosphorus sites exhibit stronger negative charge characteristics. This change is beneficial for promoting the HER process with optimal hydrogen adsorption free energy. The observed electron density decrease for Co and increase for P after Pb doping can be attributed to the higher electronegativity of Pb relative to Co, which likely causes electron transfer from Co to P. For the Pb 4f XPS spectrum in Pb-CoP/CC, the binding energies at 138.2 and 143.6 eV are attributed to the Pb $4f_{7/2}$ and Pb $4f_{5/2}$ levels of Pb^{2+} (Fig. 2d). Overall, these results confirm the successful incorporation of Pb into CoP, which modifies the electronic density of the material, increases the oxidation state of Co, and lowers the binding energy of P. This electronic structure modulation is expected to positively influence water dissociation and hydrogen adsorption during the alkaline HER process, thereby enhancing the catalytic activity of the CoP.

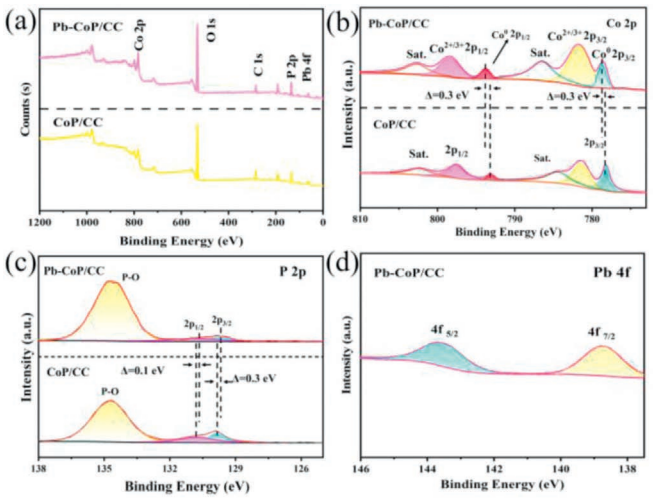


Fig. 2. (a) Full XPS spectrum of CoP/CC and Pb-CoP/CC. (b) Co 2p spectra of CoP/CC and Pb-CoP/CC. (c) P 2p spectra of CoP/CC and Pb-CoP/CC. (d) Pb 4f spectra of Pb-CoP/CC.

To investigate the HER performance of the catalysts, electrochemical tests were conducted using a three-electrode system in a 1.0 mol/L KOH solution (Fig. S6 in Supporting information). The Pb doping level was carefully optimized to improve the HER activity of Pb-CoP/CC (Fig. S7 in Supporting information). As depicted in Fig. 3a, the optimally tuned Pb-CoP/CC exhibits an overpotential of only 53 mV at 10 mA/cm^2, significantly lower than the 100 mV observed for CoP/CC, indicating its significant enhanced catalytic activity. The Tafel slopes, which are used to reveal the kinetics of the HER, are presented in Figs. 3b and c. With increasing Pb doping ratios, the Tafel slopes of the catalysts change accordingly, indicating that an appropriate amount of Pb doping can enhance the HER kinetics. Notably, the Tafel slope of $Pb_{0.03}$-CoP/CC is 57 mV/dec, significantly lower than that of the undoped CoP/CC (74 mV/dec), suggesting more favorable HER kinetics. Moreover, the Tafel slope values indicate that the HER process of Pb-CoP/CC under alkaline conditions follows the Volmer-Heyrovsky mechanism. Additionally, the turnover frequency (TOF) of the catalysts was also estimated. At an overpotential of 300 mV, the TOF value of Pb-CoP/CC is approximately nine times higher than that of CoP/CC (Fig. 3d). Although the ECSA slightly decreased, Pb doping modulates the catalyst's electronic structure and activates the active P sites, resulting in a significant increase in TOF and enhanced intrinsic catalytic activity.

To further explore the impact of Pb doping on the catalytic active area and charge transfer capability at the catalyst-electrolyte interface in CoP, double-layer capacitance (C_{dl}) measurements and electrochemical impedance spectroscopy (EIS) were performed. The electrochemical active surface area (ECSA) of the catalysts was estimated based on the C_{dl}, as the two are positively correlated (Fig. S8 in Supporting information). As shown in Fig. 3e, the C_{dl} of Pb-CoP/CC (73 mF/cm^2) is lower than that of CoP/CC (93 mF/cm^2), indicating a reduced electrochemical active surface area after Pb

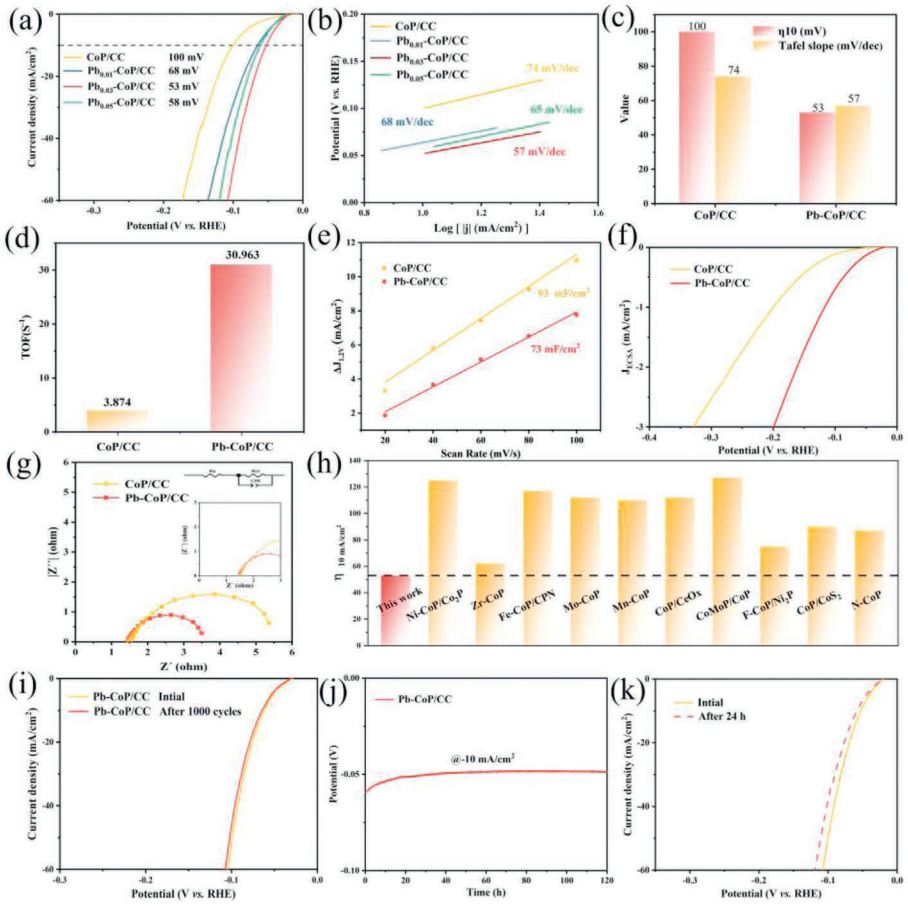


Fig. 3. (a) LSV, (b, c) Tafel curves of CoP/CC and Pb-CoP/CC. (d) TOF. (e) Double-layer capacitances. (f) Polarization curves normalized according to ECSA. (g) Nyquist plots of CoP/CC and Pb-CoP/CC. (h) Comparison of overpotential. (i) LSV curves of Pb-CoP/CC before and after 1000 cycles. (j) *V-t* curves. (k) LSV curves of Pb-CoP/CC before and after 24 h.

doping. This reduction may be attributed to the electrochemical inertness of introduced Pb, as well as the enhanced crystallinity in Pb-CoP/CC, as evidenced by the XRD results. To more accurately assess the intrinsic catalytic activity of the samples, the polarization curves were normalized by the ECSA. After normalization, the comparison of catalytic activities from the normalized polarization curves further confirms that Pb doping significantly enhances the intrinsic catalytic activity of CoP (Fig. 3f). The interfacial electron transfer capability was evaluated using EIS measurements. As shown in the Nyquist plots in Fig. 3g, Pb-CoP/CC exhibits a smaller charge transfer resistance (R_{ct}) compared to CoP/CC, indicating improved electrochemical reaction kinetics. Additionally, the similar solution resistance (R_S) values in the high-frequency region (inset in Fig. 3g) for both samples suggest that Pb doping in CoP has a negligible effect on the conductivity of the catalyst. The electrochemical measurement results above indicate that Pb doping leads to a decrease in the electrochemically active area, an increase in charge transfer capability, and a negligible change in conductivity. This suggests that the enhancement in catalytic activity is primarily attributed to an increase in the intrinsic activity of Pb-CoP/CC, which will be further validated through the following theoretical calculations and poisoning experiments. Additionally, it is worth noting that, compared to other reported CoP-based HER catalysts, our synthesized Pb-CoP/CC exhibits either superior performance or comparable efficiency (Fig. 3h and Table S2 in Supporting information).

The electrocatalyst exhibits excellent catalytic efficiency as well as strong stability. Its long-term performance was tested and verified by continuously monitoring the change in overpotential under a constant current density of $-10\,mA/cm^2$. As shown in Fig. 3i, after 1000 cycles of cyclic voltammetry (CV), the overpotential of Pb-CoP/CC at $-10\,mA/cm^2$ increased by only 4 mV. Further assessment of long-term stability was conducted using chronoamperometry at a constant current density of $-10\,mA/cm^2$, where Pb-CoP/CC demonstrated stable hydrogen evolution for at least 120 h, with minimal changes in potential (Fig. 3j). Additionally, after 24 h of cycling at $-10\,mA/cm^2$, the overpotential increased by only 8 mV, further underscoring its excellent long-term stability (Fig. 3k). Post-stability test characterizations using XRD, SEM, and XPS (Figs. S9 and S10 in Supporting information) revealed that Pb-CoP/CC retained its original crystal structure, microstructure, and surface chemical state, providing strong evidence of its exceptional electrocatalytic stability. These results collectively underscore the remarkable durability of Pb-CoP/CC, positioning it as a highly promising candidate for sustainable and long-lasting electrocatalytic applications in the alkaline HER process. Moreover, the Faradaic efficiency (FE) of Pb-CoP/CC has been verified, confirming that the observed current is indeed associated with hydrogen production. Hydrogen gas was collected *via* drainage at a current density of $10\,mA/cm^2$ (Fig. S11 in Supporting information). The FE was calculated to be approximately 99 % by comparing the theoretical hydrogen production value with the experimentally collected gas.

To investigate the impact of Pb doping on the electronic structure and hydrogen evolution reaction performance of CoP, density functional theory simulations were conducted to study the catalyst's physicochemical properties. Based on the surface

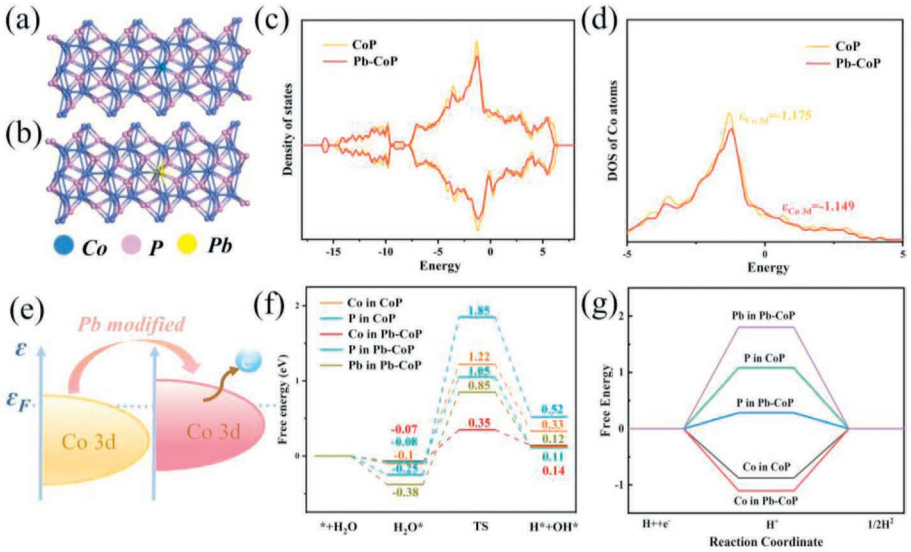


Fig. 4. (a) Schematic diagram of the crystal structure of CoP and (b) Pb-CoP. (c) Total DOS of CoP and Pb-CoP. (d) PDOS of Co atoms. (e) Schematic interaction mechanism between water HOMO and Co 3d-orbital. (f) Calculated energy barriers of H_2O dissociation kinetics of CoP and Pb-CoP. (g) Corresponding ΔG_{H^*} of CoP and Pb-CoP with different sites for HER.

morphology observed by transmission electron microscopy, the stable (112) facet of CoP was selected as the active surface for theoretical study, with its structural model shown in Fig. 4a. Pb doping was introduced by substituting the cobalt atoms exposed on the surface with lead atoms, resulting in the doped model structure illustrated in Fig. 4b. The total density of states (TDOS) for both CoP and Pb-CoP is shown in Fig. 4c. Both catalysts exhibit a continuous TDOS near the Fermi level, indicating their semimetallic nature. This conductivity is beneficial for reducing resistive polarization and promoting charge transfer during the HER reaction, thereby enhancing the reaction rate. Additionally, the similar TDOS profiles near the Fermi level for CoP and Pb-CoP indicate comparable surface conductivity, consistent with the results of the EIS tests. The position of a catalyst's d-band center is well known to correlate closely with the adsorption strength of intermediates during catalytic reactions. To analyze this, we determined the d-band center positions of the CoP and Pb-CoP catalysts through PDOS analysis (Fig. 4d). With the introduction of Pb ions, the d-band center of CoP shifts from −1.175 eV to −1.149 eV, reflecting a change in the catalyst's electronic structure and a reduction in the d-orbital electron filling, consistent with the XPS analysis described above. According to coordination theory, this upward shift of the d-band center toward the Fermi level increases the availability of empty d-orbitals on the Co center (Fig. 4e). This facilitates stronger coordination between the Co center and the highest occupied molecular orbital (HOMO) of water, leading to enhanced interaction between the Co center and water molecules [33]. The water dissociation step of the catalyst (Fig. 4f and Fig. S12 in Supporting information) reveals that, compared to pristine CoP, the Co site in Pb-CoP exhibit stronger H–O adsorption and a reduced water dissociation energy barrier. This indicates that Pb doping lowers the activation barrier for water dissociation, facilitating the formation of adsorbed hydrogen. Enhanced water dissociation plays a crucial role in accelerating the subsequent steps of the alkaline HER process, thereby significantly improving HER kinetics. This is because the dissociation of the H–O bond is widely considered the rate-determining step in HER kinetics under alkaline conditions, which also applies to CoP electrocatalysts [52]. The upward shift of the d-band center not only enhances the adsorption of water molecules but also strengthens hydrogen adsorption. However, DFT calculations indicate that Co sites exhibit strong hydrogen adsorption, making hydrogen desorption unfavorable at Co sites in Pb-doped CoP (Fig. 4g and Fig. S13 in Supporting information). Moreover, the ΔG_{H^*} value at the P sites after doping is the smallest (Fig. 4g), indicating that the P sites are activated and works as the active centers for HER in Pb-CoP. Typically, the negatively charged P sites can act as Lewis bases, effectively trapping positively charged protons during the HER process [53]. Upon Pb doping, the increased electronegativity of the P atoms enhances the properties of Pb-CoP, resulting in a Gibbs free energy for adsorbed hydrogen that approaches zero. Additionally, the near-electrocatalytic inertness observed at the Pb sites, as identified by the DFT calculations (Fig. 4g), aligns well with our initial concept of employing non-transition metal ion dopants. This calculation result further corroborates the XPS results and experimental findings. After Pb doping, the electronic structure of the catalyst is altered, and the electron distribution at the active sites is optimized, which favors the regulation of hydrogen adsorption free energy and facilitates water dissociation, thereby enhancing the HER activity. These changes enhance the water dissociation capability at Co sites and activate while optimizing H adsorption-desorption on P sites, thereby boosting alkaline HER activity.

To further confirm that the enhancement of CoP's alkaline HER activity by Pb doping is primarily due to improved water dissociation, CoP/CC and Pb-CoP/CC were evaluated under acid conditions (Fig. S14 in Supporting information). The results reveal that Pb doping has only a minor impact on the performance of CoP under acidic conditions. This indicates that the significant improvement in alkaline HER performance resulting from Pb doping is predominantly attributable to the acceleration of the water dissociation step, followed by the optimization of the H adsorption free energy. In addition, the role of P active sites was confirmed through poisoning experiments, in which 10 mmol/L KSCN and $C_{12}H_{25}SH$ were separately added to 1.0 mol/L KOH to selectively poison the Co and P sites, respectively. As shown in Fig. S15 (Supporting information), poisoning either the Co or P sites led to a significant increase in the overpotential of Pb-CoP/CC at 10 mA/cm^2, rising from the initial 53 mV to 92 mV and 117 mV, respectively. Notably, the performance deteriorated more substantially when the P sites were poisoned, underscoring the dominant role of P sites in the HER process. Therefore, the exceptional alkaline HER activity of Pb-CoP/CC can be attributed to the synergistic effect of electronic structure modulation at both Co and P sites, as demonstrated by experimental evidence and DFT calculations.

To assess the feasibility of Pb-CoP/CC for large-scale hydrogen production, a flow-type anion exchange membrane (AEM) electrolyzer was assembled. Pb-CoP/CC was used as the cathode, while a commercially available IrO_2-coated platinum-titanium felt served as the anode (Figs. S16a and b in Supporting information). The steady-state polarization curve demonstrates that under operation at 60 °C with 1.0 mol/L KOH in the flow electrolyzer, the Pb-CoP||IrO_2 system achieved current densities of 100 and 500 mA/cm^2 at applied voltages of 1.28 and 1.95 V, respectively (Fig. S17 in Supporting information). This performance surpasses that of CoP/CC, indicating that the incorporation of Pb significantly enhances the overall water-splitting efficiency. However, compared to the commercial Pt/C||IrO_2 system (1.32 V@100 mA/cm^2, 1.84 V@500 mA/cm^2), the performance of Pb-CoP/CC at higher current densities still requires further improvement. Long-term stability tests (Fig. S18 in Supporting information), reveal that the Pb-CoP/CC-based electrolyzer maintained excellent AEM electrolyzer performance over 100 h of operation at 500 mA/cm^2 and 60 °C, significantly outperforming both traditional CoP/CC and commercial Pt/C in durability. These results highlight the strong potential of Pb-CoP/CC as a stable and efficient catalyst for industrial-scale hydrogen production, underscoring its practicality for sustainable energy applications.

In summary, we have demonstrated that Pb doping significantly enhances the catalytic performance of CoP nanowires for the HER in alkaline media, addressing the long-standing challenges of improving water dissociation kinetics and optimizing hydrogen adsorption. The optimized Pb-CoP/CC catalyst demonstrates outstanding performance, achieving a low overpotential of 53 mV at 10 mA/cm^2, a Tafel slope of 57 mV/dec, and excellent long-term stability. This improvement stems from the synergistic effects of Pb doping, which regulates the electronic structure of both the Co and P sites. This not only accelerates water dissociation but also optimizes hydrogen intermediate adsorption and enhances charge transfer capabilities. Theoretical studies further corroborate these findings, revealing that Pb doping effectively modulates the electronic structure of CoP. This modulation promotes water dissociation at Co sites and facilitates hydrogen adsorption at P sites during the HER process. When integrated into AEM electrolyzer, the Pb-CoP/CC catalyst demonstrates outstanding performance, delivering a current density of 500 mA/cm^2 at a cell voltage of 1.95 V, underscoring its potential for industrial-scale hydrogen production. Our results not only highlight the effectiveness of non-transition metal doping in modifying the electronic structures of transition metal-based compounds but also offer a versatile strategy for enhancing the performance of non-precious metal catalysts. This work offers a promising pathway for the development of high-performance, cost-effective electrocatalysts for AEM electrolyzers, paving the way for large-scale green hydrogen production.

CRediT authorship contribution statement

Shiqing Zhang: Writing – original draft, Formal analysis, Data curation. **Zihao Wang:** Methodology, Investigation. **Shaokai Ma:** Investigation. **Zihang Cao:** Methodology, Investigation. **Fang Liu:** Software. **Ying Li:** Software, Resources. **Xuewen Xu:** Validation. **Yuanhui Ma:** Resources. **Yanming Xue:** Visualization, Resources. **Chengchun Tang:** Funding acquisition. **Jun Zhang:** Writing – review & editing, Supervision, Funding acquisition, Conceptualization.

Declaration of competing interest

The authors declare that they have no known competing financial interests or personal relationships that could have appeared to influence the work reported in this paper.

Acknowledgments

The authors gratefully acknowledge the financial support from the Natural Science Foundation of Hebei Province (Nos. E2024202067 and E2021202121). This work is also supported by the Program for the Outstanding Young Talents of Hebei Province and S&T Program of Hebei (No. 22567602H), China.

Supplementary materials

Supplementary material associated with this article can be found, in the online version, at doi:10.1016/j.cclet.2025.111785.

References

[1] K. de Kleijne, M.A.J. Huijbregts, F. Knobloch, et al., Nat. Energy 9 (2024) 1139–1152.
[2] T. Longden, F.J. Beck, F. Jotzo, et al., Appl. Energy 306 (2022) 118145.
[3] L. Wang, D. Wang, L. Zheng, et al., Nano Res. 17 (2024) 9472–9482.
[4] L. Zhang, J. Li, M. Hu, et al., Chin. Chem. Lett. 36 (2025) 111123.
[5] M. Chatenet, B.G. Pollet, D.R. Dekel, et al., Chem. Soc. Rev. 51 (2022) 4583–4762.
[6] L. Chen, Q. Xu, S.Z. Oener, et al., Nat. Commun. 13 (2022) 3846.
[7] D. Henkensmeier, W.C. Cho, P. Jannasch, et al., Chem. Rev. 124 (2024) 6393–6443.
[8] F. Rocha, C. Georgiadis, K. Van Droogenbroek, et al., Nat. Commun. 15 (2024) 7444.
[9] Y. Liu, X. Sun, Y. Wang, et al., Chem. Eng. J. 493 (2024) 152644.
[10] W. Wu, X. Ma, Y. Zhu, et al., Chem. Eng. J. 478 (2023) 147425.
[11] A.A. Feidenhans'l, Y.N. Regmi, C. Wei, et al., Chem. Rev. 124 (2024) 5617–5667.
[12] B. Li, T. Wang, M. Xu, et al., Chin. Chem. Lett. 36 (2025) 110467.
[13] S. Zhu, X. Liu, X. Wang, et al., Joule 8 (2024) 1890–1918.
[14] P.C.K. Vesborg, T.F. Jaramillo, RSC Adv. 2 (2012) 7933–7947.
[15] Z. Chen, X. Duan, W. Wei, et al., J. Mater. Chem. A 7 (2019) 14971–15005.
[16] J. Mohammed-Ibrahim, X. Sun, J. Energy Chem. 34 (2019) 111–160.
[17] Y. Wang, H. Arandiyan, S.S. Mofarah, et al., Adv. Mater. 36 (2024) 2402156.
[18] N.K. Mahale, S.T. Ingle, Energy 119 (2017) 872–878.
[19] J. Li, L. Wang, H. He, et al., Nano Res. 15 (2022) 4986–4995.
[20] J. Pan, X. Liu, H. Ji, et al., Chin. Chem. Lett. 35 (2024) 109515.
[21] J. Greeley, J.K. Nørskov, L.A. Kibler, et al., ChemPhysChem 7 (2006) 1032–1035.
[22] B. Wang, F. Yang, L. Feng, Small 19 (2023) 2302866.
[23] L.A. King, M.A. Hubert, C. Capuano, et al., Nat. Nanotechnol. 14 (2019) 1071–1074.
[24] P. Liu, J.A. Rodriguez, J. Am. Chem. Soc. 127 (2005) 14871–14878.
[25] X. Huang, X. Xu, X. Luan, et al., Nano Energy 68 (2020) 104332.
[26] L. Ji, J. Wang, X. Teng, et al., ACS Catal. 10 (2020) 412–419.
[27] W. Zhang, N. Han, J. Luo, et al., Small 18 (2022) 2103561.
[28] F.H. Saadi, A.I. Carim, E. Verlage, et al., J. Phys. Chem. C 118 (2014) 29294–29300.
[29] D.H. Ha, B. Han, M. Risch, et al., Nano Energy 29 (2016) 37–45.
[30] G.H. Gao, R.Z. Zhao, Y.J. Wang, et al., Chin. Chem. Lett. 35 (2024) 109181.
[31] G. Huang, Y. Huang, A. Ali, et al., Electron 2 (2024) e58.
[32] K. Xu, H. Ding, M. Zhang, et al., Adv. Mater. 29 (2017) 1606980.
[33] Y. Men, Y. Tan, P. Li, et al., Appl. Catal. B: Environ. 284 (2021) 1119718.
[34] Q. Wang, R. He, F. Yang, et al., Chem. Eng. J. 456 (2023) 141056.
[35] Y. Men, P. Li, J. Zhou, et al., Cell Rep. Phys. Sci. 1 (2020) 100136.
[36] K. Jang, H. Yoon, J.S. Hyoung, et al., Appl. Catal. B: Environ. 341 (2024) 123327.
[37] Y. Zhao, N. Dongfang, C.A. Triana, et al., Energy Environ. Sci. 15 (2022) 727–739.
[38] G. Huang, M. Hu, X. Xu, et al., Small Struct. 4 (2023) 2200235.
[39] W. Xu, G. Fan, S. Zhu, et al., Adv. Funct. Mater. 31 (2021) 2107333.
[40] X. Cao, Y. Tan, H. Zheng, et al., Phys. Chem. Chem. Phys. 24 (2022) 4644–4652.
[41] R. Li, P. Ren, P. Yang, et al., Nano Energy 126 (2024) 109613.
[42] X.Z. Song, W.Y. Zhu, J.C. Ni, et al., ACS Appl. Mater. Inter. 14 (2022) 33151–33160.
[43] H. Jin, X. Liu, S. Chen, et al., ACS Energy Lett. 4 (2019) 805–810.
[44] X. Liu, B. Wei, R. Su, et al., Energy Technol. 7 (2019) 1900021.
[45] X. Wang, Y. Chen, B. Yu, et al., Small 15 (2019) 1902613.
[46] W. Liu, K. Jiang, Y. Hu, et al., J Colloid Interface Sci. 604 (2021) 767–775.
[47] H. Fan, D. Jiao, J. Fan, et al., J. Energy Chem. 83 (2023) 119–127.
[48] R. Zhang, C. Tang, R. Kong, et al., Nanoscale 9 (2017) 4793–4800.
[49] Y. Wang, X. Sun, Y. Liu, et al., Fuel 357 (2024) 129825.
[50] F. Liu, W. He, Y. Li, et al., Appl. Surf. Sci. 546 (2021) 149101.
[51] F. Yang, Y. Chen, G. Cheng, et al., ACS Catal. 7 (2017) 3824–3831.
[52] Y. Men, P. Li, J. Zhou, et al., Cell Rep. Phys. Sci. 1 (2020) 100136.
[53] J. Cai, Y. Song, Y. Zang, et al., Sci. Adv. 6 (2020) 8113.